Analysis On The Regional Features of Future Warming Using High-Resolution Downscaled Multi-Model Climate Scenarios In China

Lei Zhang
National Meteorological Center
Yinlong Xu (xuyinlong@caas.cn)
Chinese Academy of Agricultural Sciences
Chunchun Meng
China Meteorological Administration
Yuncheng Zhao
Chinese Academy of Agricultural Sciences
Changgui Wang
JBA Consulting, Pipe House, Lipton Rd

Research Article

Keywords: Future warming, freezing-event, heat-stress event, downscaled climate models

Posted Date: November 3rd, 2021

DOI: https://doi.org/10.21203/rs.3.rs-906550/v1

Abstract

The frequency and magnitude of global warming events varies greatly across different regions and countries. The climatic diversity for China and future warming features are projected across twelve climatic zones based on the ensemble of the five well-performing high resolution downscaled climate models for each zone. There are warming patterns for the mean near surface air temperature (Tm), maximum near surface air temperature (Tmax), minimum near surface air temperature (Tmin) as well as heat stress and frost events. Under RCP4.5 and RCP8.5 scenarios, the three indices (i.e., Tm, Tmax and Tmin) countrywide are likely to increase at respective rates of 0.30-0.31 and 0.64-0.67 ^{o}C per decade. The extent of freezing-event extent (FE) are projected to decrease at a rate of -1912 and -4442 day·km^2 per decade while the extent of heat-stress event (HE) increase at 1116 and 3557 day·km^2 per decade. A higher increment in temperatures as well as a decreasing trend in the diurnal temperature range (DTR) and frost days and FE are present on the Tibetan Plateau and northern China including Xinjiang, Northeast China, the eastern part of northwest China, Inner Mongolia and North China. These trends are opposite to those projected for southern China including Huanghuai, Jianghuai, Jianghan, the south Yangzi River, South China and Southwestern China. The warming occur faster in the current colder zones (northern China and the Tibetan Plateau) while heat stress is more intense and severe in Jianghuai, Jianghan, the south Yangzi River, South China and Xinjiang. These potential changes indicate that adaption and mitigation strategies are necessary in response to future warming.

1 Introduction

There is broad agreement that global warming has increased by 0.85 ^{o}C in temperature records from 1880 to 2012 (IPCC 2013). This mean trend in warming also corresponds to decreases in cold and increases in warm extremes over the major global land masses since the mid-20th century (IPCC 2013). These events are also reflected in a smaller value for the global diurnal temperature range (DTR) due to unsynchronized variations in maximum and minimum temperatures (IPCC 2013). These types of diverse spatial patterns are apparent globally and more significant in particular regions of the globe such as the eastern United States, northern Europe, western Africa and East Asia (IPCC 2014). Large parts of Europe, Asia and Australia are experiencing increased extreme warm events that have already led to catastrophic consequences such as forest fires in the Amazon and Australia in 2019 and locust outbreaks in East Africa in 2020.

China has a diverse geography that is associated with a record of 0.9–1.5 ^{o}C increase in its average temperature from 1909 to 2011 (China's Third National Assessment Report on Climate Change, 2015). The DTR is also decreasing at a rate of -0.04 to -0.20°C per decade as calculated using data from 1951 to 2014 (Sun et al. 2019). In terms of regional characteristics, there have been increasing temperatures and decreasing DTR in northern China (Zhang et al. 2011; Wang et al. 2017c; Shi et al. 2019), more frequent and intense heatwaves in mid-eastern China (Huang et al. 2018) and decreased frost events overall but particularly in northern China (Guo et al. 2019).

Skillful projections of future climatic trends are vital for an understanding of the causes and potential mitigation and adaptation strategies for climatic alterations. Over the past ~ 30 years, different greenhouse gas (GHG) emission scenarios has been developed, including the Intergovernmental Panel on Climate Change scenarios published in 1992 (IS92; IPCC, 1992), the Special Report for Emission Scenarios (SRES; IPCC, 2007), the Representative Concentration Pathways (RCP; IPCC, 2013) up to the present Shared Socio-Economic Pathway (SSP; IPCC, 2019). General temperature features have been extensively explored under these scenarios for China (Tian et al. 2015; Wang et al. 2015; Bannister et al. 2018). A warming of 1–3 ^{o}C is projected over China in the 21st century under the SRES B1, A1B and A2 scenarios with larger magnitudes in northern China (Chen et al. 2011; Jiang et al. 2009, 2012). Recently, characteristics of temperature increments have been analyzed under RCP scenarios (Zhao et al. 2016; Wang et al. 2017b; Huang et al. 2018) and these projections indicated that the national average temperature respectively increases by 0.76, 1.84 and 2.10 ^{o}C in the periods 2017–2036, 2046–2065 and 2080–2099 under RCP4.5 (Guo et al. 2018b), as well as 5.7 ^{o}C in 2070–2099 under RCP8.5 (Zhu et al. 2017). Global climate model (GCM) simulations are diverse in their GHG emissions scenarios and can provide general acceptable results particularly worldwide or nationwide. However, these can not meet the demand of many impacts related studies at the regional or local scale, due to their coarse resolution (Yue et al. 2016; Marotzke et al. 2017). A series of statistical downscaling (SD) methods and dynamical downscaling ways (DD, i.e., regional climate model) have thus been applied to these models to produce high-resolution climate scenario datasets that account for average and extreme temperature alterations (Zhu et al. 2013; Gao et al. 2017; Liang et al. 2019; Niu et al. 2018; Zhou et al. 2018). These works have demonstrated that SD and DD are more robust in performance of the characteristics of regional and local climatic features. In addition, more skillful projections can be obtained from finer-resolution outputs although there is still inconsistent performance in sub-regions such as a cold bias for eastern and northwestern China (Ji and Kang 2015) and poor simulation in reproducing spatial patterns of extreme temperatures in western China (Zhu et al. 2017; Guo et al. 2018a; Zhai et al. 2019). The primary reason for these discrepancies is that bias corrections between outputs from models and observations have been inevitable (Guo et al 2018b).

The whole of mainland China is divided into several climatic zones according to regional characteristics (Huang et al. 2018). In particular, the annual average temperatures for the Tibetan Plateau and northern China have been greater than in the east and south (Tian et al. 2015). A negative DTR trend and larger reductions of frost days have been demonstrated in Tibetan Plateau (Yang et al. 2014; You et al. 2017) along with heatwaves in the central and eastern regions (Huang et al. 2018; Lin et al. 2018). However, a systematic exploration that includes these regional features for future warming is still lacking and a more complete scientific understanding of regional future warming trends is needed especially based on more accurate and finer-resolution multi-model climate projections processed using SD and DD. The purpose of this study is to unveil the potential spatial-temporal features of temperatures for the 21st century across different climatic zones over mainland China based on an ensemble of the five well-performing SD or DD outputs for each zone. Changes of mean temperature, maximum and minimum temperatures as well as the DTR are analyzed for mean warming trends and frost and heatwaves are quantified at a regional scale to reveal extreme temperature trends.

The structure of this study is organized as follows: (Sect. 2) brief descriptions of the study region, model datasets, analytic methods and emphatic points; (Sect. 3) results related to future regional changes of average and extreme temperatures under RCP4.5 and RCP8.5 scenarios; (Sect. 4) analysis of the

reliability of the associated methods and findings and (Sect. 5) a summary of the primary results.

2 Material And Methods

2.1 Study region and datasets

The diverse geography of China includes multiple land types and atmospheric circulation systems responsible for differing climatic conditions for China. The whole of mainland China is divided into 12 climatic zones (Huang et al. 2018) as follows: Northeast China (NE), North China (NC), Inner Mongolia (IM), Huanghuai (HH), Xinjiang (XJ), the eastern part of northwest China (WE), Jianghuai (JH), Jianghan (JHa), the south Yangzi River (SY), South China (SC), Southwestern China (SW) and the Tibetan Plateau (TP) (Fig. 1).

The climate scenarios datasets used for the analyses in this paper contain those generated from twenty GCMs (Table S1) from the Coupled Model Intercomparison Project Phase 5 and one regional climate model named Providing Regional Climates to Impact Studies (PRECIS, version 2.1) (Xu et al. 2006; Yang et al. 2010; Zhang et al. 2017; Li et al. 2018). The daily simulations extend from the years 1961 to 2100, and the historical observations for the period of 1961–2005 are used for model validation and calibration.

2.2 Statistical downscaling for GCMs and bias correction for PRECIS outputs

Since local climate features cannot be reflected from the coarse GCM resolutions, we apply the statistical downscaling method named Bias Correction Spatial Disaggregation (BCSD) to the daily GCM outputs. The BCSD is appropriate for its effective capture of biased statistical characteristics and direct implementations to the daily outputs (Bürger et al. 2012). The BCSD (Ning et al. 2015; Werner and Cannon 2015) utilizes quartile mapping to correct the bias between raw GCM outputs and then interpolates the adjusted scaling factors to generate fine-resolution ($0.25^o \times 0.25^o$) outputs, which detailed algorithm is described in previous work (Zhang et al. 2020). For PRECIS, it is appropriate for using the same quartile mapping bias correction procedure to correct the bias between PRECIS outputs and observation.

2.3 Temperature indices

The terms Tm, Tmax, Tmin and DTR are employed to describe the mean trends of spatial-temporal warming features. Heatwaves and frost are of particular interest as these extreme events have significant impacts on human communities, agroecosystems and socio-economic development (Jones et al. 2015; Kukal and Irmak 2018; Liu et al. 2018). Therefore, four indices, i.e., heat stress days (HD), frost days (FD), the extent of heat-stress event (HE) and the extent of freezing event (FE) are as constructed as follows:

$$HE = HD \times S_{HD} \quad (1)$$

$$FE = FD \times S_{FD} \quad (2)$$

where HD is the number of days with daily Tmax greater than 35 ^oC in one year; FD is the number of days with daily Tmin less than 0 ^oC in one year; HE and FE are regional extent indices calculated by multiplying the mean value of HD or FD and the area (with the unit of km^2) of grids (S_{HD} or S_{FD}) exposed to heat stress or frost in a specific zone.

The time periods, 2031–2060 (P1) and 2071–2100 (P2), are chosen to represent the mid- and late- 21st century for the analysis of temperature change features *via* comparisons with the baseline period 1961–1990 (P0). The Thiel-Sen method (Thiel 1950; Sen 1968) with no limitation of the influence of the outliers on the slop, is used to evaluate trends for these variables as follows:

$$Ts = median\left[\frac{x_j - x_i}{j - i}\right] \quad \{i < j\} \quad (3)$$

where x_i and x_j are the sequential data values of time i and j in the time series, Ts is the estimated magnitude for the variables.

The performances that are presented in the simulations used with statistical downscaled GCMs and bias corrected PRECIS are different in reflecting regional temperature projections. The top five well-performing models (Table S2) are selected for each zone as described previously (Zhang et al. 2020), by the metric of a comprehensive ranking index coupled of the spatial correlation coefficient, the root-mean-square error, standard deviations and symmetrical uncertainty. An ensemble of the top five well-performing models for each zone is utilized to maximize the regional robustness of the models (Xu et al. 2010; Xu et al. 2013).

3 Results

3.1 Potential warming features of average temperatures

The values for Tm, Tmax and Tmin relative to the period 1961–1990 are projected to increase across all regions of China and the increments increase from southeast to northwest. These trends include representative warming of 6.3 and 5.1 ^oC in XJ and TP for Tm, 6.2 and 5.6 ^oC for Tmax, 5.7 and 6.5 ^oC for Tmin from 2071–2100 under RCP8.5 (Figs. 3 and 4). The national average trend of Tm, Tmax and Tmin in the period 2006–2100 reach 0.30, 0.30 and 0.31 ^oC per decade under RCP4.5, 0.64 and 0.65 and 0.67 ^oC per decade under RCP8.5, respectively (Fig. 4 and Table 1). The tendency of maximum Tmax (yearly

maximum value of Tmax) under RCP4.5 and RCP8.5 is 0.01 and 0.02 ^{o}C per decade higher than Tmax, and the minimum Tmin (yearly minimum value of Tmin) is 0.05 and 0.09 ^{o}C per decade higher than Tmin, respectively. These data are consistent with lower base values but higher increments for Tm, Tmax and Tmin for XJ, TP, NE, WE, IM and NC while a higher value but lower increment is projected for SC, SY, JH, JHa, SW and HH (Fig. S1-S3).

The DTR will not obviously vary during different periods (Figs. 5 and S4) and spatial comparisons for 2031–2060 and 1961–1990 illustrate that DTR increases in western XJ, southern NC, HH, JH, JHa, SY, SC, SW and central and northeastern TP where Tmax increases faster than Tmin (Fig. 6). Relative to 2031–2060, the DTR for 2071–2100 under RCP8.5 decreases for NE but increases in the central regions (i.e., HH, JH, JHa, northern SY and northern SW). These projections are less apparent using RCP4.5. Overall, a smaller DTR is detected for HH, JH, JHa, SY, SC and SW in which an upward trend in DTR is also projected (Table 1 and Fig. S4).

Table 1
Thiel-Sen results for Tm/Tmax/Tmin/DTR/FD/HD in different periods (P0, P1 and P2 represent 1961–1990, 2031–2060 and 2071–2100, respectively; unit is

	P0	2006 ~ 2100-RCP4.5	2006 ~ 2100-RCP8.5	P1-RCP4.5	P2-RCP4.5	P1-RCP8.5	P2-RCP8.5
China	0.017,0.016,0.019,	0.030,0.030,0.031,	0.064,0.065,0.067,	0.035,0.037,0.034,	0.008,0.008,0.006,	0.065,0.065,0.065,	0.074,0.071
	-0.003,-0.161,0.027	0.001,-0.235,0.133	0.003,-0.530,0.395	0.003,-0.271,0.177	0.002,-0.060,0.047	0.006,-0.528,0.351	0.010,-0.592
HH	0.011,0.009,0.014,	0.029,0.031,0.028,	0.061,0.063,0.041,	0.036,0.039,0.029,	0.004,0.005,0.006,	0.060,0.061,0.060,	0.071,0.073
	-0.005,-0.18,-0.003	0.003,-0.309,0.279	0.008,-0.481,0.305	0.010,-0.284,0.436	-0.001,-0.102,0.093	0.001,-0.826,0.662	0.004,-0.761
JHa	0.012,0.012,0.012,	0.029,0.031,0.0270,	0.061,0.064,0.041,	0.036,0.04,0.029,	0.003,0.003,0.004,	0.059,0.061,0.057,	0.068,0.071
	0.001,-0.104,0.037	0.004,-0.275,0.302	0.007,-0.528,0.384	0.013,-0.253,0.468	0.002,-0.047,0.062	0.007,-0.592,0.750	0.006,-0.419
SC	0.009,0.012,0.009,	0.026,0.026,0.025,	0.052,0.053,0.040,	0.032,0.035,0.029,	0.008,0.011,0.006,	0.055,0.058,0.054,	0.057,0.056
	-0.001,-0.02,0.033	0.003,-0.017,0.375	0.003,-0.044,0.487	0.006,-0.014,0.54	0.005,-0.004,0.094	0.004,-0.035,1.019	-0.002,-0.01
SY	0.009,0.008,0.009,	0.028,0.029,0.026,	0.057,0.06,0.039,	0.032,0.036,0.028,	0.007,0.008,0.006,	0.059,0.063,0.056,	0.063,0.066
	-0.002,-0.091,0.019	0.004,-0.132,0.31	0.005,-0.303,0.426	0.009,-0.147,0.454	0.003,-0.017,0.117	0.007,-0.281,0.784	0.005,-0.151
SW	0.008,0.009,0.009,	0.027,0.028,0.026,	0.056,0.058,0.040,	0.033,0.036,0.031,	0.007,0.009,0.005,	0.058,0.061,0.056,	0.063,0.066
	-0.001,-0.057,0.006	0.003,-0.151,0.095	0.001,-0.307,0.103	0.008,-0.167,0.134	0.004,0.009,0.062	0.006,-0.332,0.262	0.005,-0.186
WE	0.015,0.017,0.016,	0.031,0.030,0.032,	0.064,0.064,0.045,	0.036,0.037,0.034,	0.005,0.007,0.004,	0.063,0.062,0.065,	0.074,0.073
	-0.001,-0.143,0.007	-0.001,-0.279,0.084	0.001,-0.406,0.071	0.003,-0.321,0.111	0.001,-0.06,0.003	-0.003,-0.807,0.222	-0.005,-0.98
NE	0.019,0.018,0.021,	0.031,0.030,0.031,	0.068,0.065,0.052,	0.034,0.034,0.033,	0.007,0.006,0.006,	0.063,0.061,0.064,	0.082,0.074
	-0.003,-0.132,0.004	-0.001,-0.194,0.044	-0.006,-0.315,0.035	0.001,-0.204,0.052	0.001,-0.021,0.014	-0.004,-0.643,0.109	-0.015,-0.86
IM	0.021,0.018,0.022,	0.033,0.034,0.031,	0.067,0.065,0.050,	0.033,0.035,0.032,	0.006,0.006,0.006,	0.064,0.063,0.064,	0.079,0.073
	-0.003,-0.146,0.027	-0.001,-0.197,0.105	-0.006,-0.297,0.108	0.001,-0.206,0.142	0.001,-0.017,0.029	-0.003,-0.67,0.255	-0.010,-0.87
NC	0.015,0.013,0.019,	0.030,0.031,0.029,	0.063,0.063,0.042,	0.033,0.034,0.031,	0.009,0.009,0.009,	0.061,0.061,0.061,	0.075,0.074
	-0.004,-0.138,-0.004	0.001,-0.244,0.168	0.004,-0.352,0.147	0.004,-0.242,0.206	-0.001,-0.089,0.048	-0.003,-0.779,0.388	-0.004,-0.96
XJ	0.024,0.025,0.025,	0.032,0.032,0.032,	0.069,0.069,0.050,	0.042,0.043,0.041,	0.004,0.004,0.004,	0.072,0.068,0.069,	0.081,0.076
	-0.002,-0.176,0.11	0.001,-0.253,0.217	-0.002,-0.368,0.317	0.001,-0.324,0.27	0.001,-0.049,0.047	-0.001,-0.721,0.554	-0.005,-1.05
JH	0.009,0.009,0.012,	0.029,0.030,0.027,	0.059,0.062,0.039,	0.034,0.039,0.028,	0.001,-0.002,0.003,	0.061,0.062,0.059,	0.068,0.072
	-0.003,-0.129,0.007	0.003,-0.230,0.313	0.007,-0.433,0.365	0.011,-0.220,0.505	-0.002,-0.011,0.069	0.004,-0.554,0.738	0.007,-0.398
TP	0.017,0.015,0.018,	0.032,0.032,0.032,	0.069,0.068,0.048,	0.037,0.038,0.038,	0.008,0.012,0.007,	0.071,0.072,0.073,	0.075,0.071
	-0.003,-0.256,0.002	-0.001,-0.373,0.006	-0.001,-0.574,0.006	0.001,-0.422,0.007	0.004,-0.117,0.003	-0.001,-0.946,0.014	-0.013,-1.42

3.2 Potential warming features of extreme temperature events

Spatial comparisons also demonstrate that the FD for 2031–2060 under RCP4.5 relative to 1961–1990 shrink by 20–40 days for TP, HH, JH, JHa and southern WE while FD is much shorter in most regions under RCP8.5. There is a general shrinkage of < 10 days and 5–50 days across the whole country under RCP4.5 and RCP8.5 for 2071–2100, respectively (Fig. 7). The decreasing rate of FD at the national level is calculated as -2.35 and − 5.30 days per decade during 2006–2100 under RCP4.5 and RCP8.5, respectively (Fig. 8 and Table 1). This is the most obvious for FD in TP with a respective rate of -3.73 and − 5.74 days per decade under RCP4.5 and RCP8.5 (Table 1). Comparisons of regional FD between 2071–2100 and 1961–1990 illustrate that the decrement under RCP8.5 is > 42 days for WE, NE, IM, NC, XJ and TP, twice as much as the decrement under RCP4.5 (Fig. 9). The regional intensities indicate the countrywide FI decreases from 1.63×10^5 day·km^2 (1961–1990) to 1.39×10^5 day·km^2 and 1.22×10^5 day·km^2 (2071–2100) under RCP4.5 and RCP8.5, respectively. The

tendency of the countrywide FE is -4442 day·km^2 per decade for 2006–2100 under RCP8.5, more than twice that calculated under RCP4.5 (-1912 day·km^2 per decade). It is clear that the decreasing trend in FE is present for TP, XJ, IM, NE, WE and NC, though these values are still high (Fig. 10).

The HD for 2031–2060 under RCP4.5 relative to 1961–1990 increases by 25–35 days in southern XJ, 15–30 days in southeastern NC, central-western HH, JH, JHa, SY, SC and northeastern SW while the increment is less under RCP8.5 (Fig. 7). In 2071–2100 relative to 2031–2060, there is a increment of 10–25 days under RCP4.5 in central-eastern regions and southern XJ and 30–75 days under RCP8.5. The countywide HD is likely to increase at a rate of 3.95 days per decade for 2006–2100 under RCP8.5, nearly three times as much as that under RCP4.5 (Fig. 8 and Table 1). Regional comparisons of HD between 2071–2100 and 1961–1990 indicate that the increment is > 52 days in SY, SC, JH, JHa and HH under RCP8.5 and > twice that under RCP4.5 (Fig. 9). The HE ranges from 0.32×10^4 day·km^2 in 1961–1990 to 1.39×10^4 and 3.00×10^4 day·km^2 in 2071–2100 under RCP4.5 and RCP8.5, respectively (Fig. 11). There is an increasing trend for HE at a rate of 3557 day·km^2 per decade under RCP8.5 that is > 3 times that calculated under RCP4.5 (1116 day·km^2 per decade) and > 7 times the baseline (455 day·km^2 per decade). It is obvious that higher values and increasing trends for HE are demonstrated in XJ, SY and SC. In particular, the tendency of FI in XJ is 346 and 886 day·km^2 per decade for RCP4.5 and RCP8.5, nearly twice as much as that for SY and SC.

4 Discussion

Based on the optimal ensemble of top five well-performing bias-corrected climate models, we project the potential features of future warming across mainland China. In general, there are homogeneous increases for Tm, Tmax, Tmin and HD and decrease for FD under RCP4.5 and RCP8.5 scenarios modeling. Comparisons between these scenarios elucidate future increasing warming trends and more significant increments are projected under RCP8.5 and correlate well with potential GHG emission assumptions. Larger increments are found for Tm, Tmax and Tmin in the northern and western zones, which is consistent with previous findings (Zhang et al. 2011; Zhou et al. 2014; Chen and Frauenfeld 2014; Tian et al. 2015). The probabilities for Tm values with increments > 4.0 ^{o}C for 2070–2099 relative to 1961–1990 are calculated at 60 % for the regions NE, XJ, WE and TP. This is higher than other regions in China as predicted under the SRES A1B scenario (Chen et al. 2011). The strongest warming trend has been projected for the higher latitudes and high-elevation areas under RCP4.5 and RCP8.5 (Xu et al. 2019) and future increases in the magnitude of Tm, Tmax and Tmin are consistently greater in northern China (Guo et al. 2018b) as well as inland areas of the northwest (Wang and Chen 2014). Overall, These studies predict a homogenous warming in western and northeastern China and are similar to the findings in the current study. These results are also consistent with radiative flux approximations where higher downward longwave and shortwave radiation decrease while upward shortwave radiation increases in southern zones leading to a lower temperature increase (Chen and Zhou 2016). However, the warming magnitudes derived from these previous studies and our projection are unequal and can be attributed to differences in selected models, scenarios and downscaling and bias correction processes.

Tmax and Tmin also display inconsistent increases that led to distinctive patterns for the DTR. A consistent DTR decreasing trend for 1961–1990 is demonstrated for NE, IM, NC, WE and XJ. This has been previously attributed to the greater increments for Tmin than Tmax (Wang et al. 2017b; Shi et al. 2019). In future periods, Tmax rarely increases faster than Tmin in the northern and western zones and is attributed to evaporation increases and decreases in soil moisture affected by warming (Russo and Strel 2011). In addition, widespread significant warming trends have been predicted for all temperature-related extreme indices except for DTR across the Loess Plateau (Wang et al. 2017a). This is also consistent with the unobvious trend for DTR across WE found in the current study.

The metrics of extremes are also presented in the current study to illustrate potential alterations for heat waves and frost under climate warming because they are closely linked to human communities, ecosystems and regional economic development (Jones et al. 2015; Kukal and Irmak 2018; Liu et al. 2018). Generally, FD is projected to decrease in the future, which strongly concurs with other similar studies that modeled the responses of cold extremes to warming (Yang et al. 2014; Guo et al. 2018a). It is projected that FD gradually shorten in the middle and late 21st century, with larger decreases in TP and marginal areas of the southwest but smaller changes in the southern regions (Guo et al. 2018a; Guo et al. 2018b; Yang et al. 2014). These projections match the projections found in the current work. The projected decrement of FD for 2070–2099 relative to 1961–1990 is likely to be 25.7 days under RCP4.5 and 45.6 days under RCP8.5 (Xu et al. 2018). This is a bit different to our projected decrement and might have resulted from the differential selection of models and methods. Contrary to FD, HD increases across China under warming with a larger increment in the eastern and southern regions and is consistent with previous studies that reveal eastern and southern China tend to be more sensitive to increases in warm extremes (Huang et al. 2018; Xu et al. 2018). A record hot summer is observed in eastern China in 2013 and the frequency of similar heat events is projected to increase by 16 and 33 times when global warming is at the level of 1.5 and 2°C, respectively (Lin et al. 2018). Specifically, the tendency of HD in 2071–2100 under RCP4.5 is larger than 1961–1990 while the tendency of Tmax is lower due to the larger incremental magnitudes in extreme Tmax. We additionally analyze FE and HE and find regional intensity of heat and frost events that can provide quantitative comparisons and highlighted the heat-sensitive zones. The changes in heat and frost events are primarily confined to the zones threatened by the extremes suggesting an ongoing threat should be expected in these zones.

A benefit of climate warming is that it can promote effective utilization of potential thermal resources such as prolongation and a northern shift of growing season (Zhang et al. 2014; Li et al. 2015). However, some negative reactions are inevitable such as an overall negative impact on crop yields if no appropriate remediation measures are taken (Challinor et al. 2014; Zhao et al. 2016). It should be emphasized that frost is likely to occur on some days across some parts in future period, although there is a general decrease in FD. Previous studies have concluded that the length of frost duration during growing seasons lengthen in many areas at latitudes > 30°N although climate warming reduces the total number of frost days (Liu et al. 2018). A larger increment of HD is projected around the eastern and southern regions where the agricultural production dominates China's food security. Following more frequent heat waves, rice will be threatened by more severe heat stress along the Yangtze River (Zhang et al. 2018). In addition, higher intensity of population in eastern and southern regions implies that heat stress has posed a threat on human outdoor activities, health and eventual mortality as well as morbidity (Fischer and Knutti 2013; Sylla et al. 2018; Li et al. 2018b). Better insights into these characteristics can enable us to conduct a better adjustment to climate change, especially those relief measures over high exposure regions.

Gridded and shaded areas derived from Figs. 4 and 9 indicate that bias corrected values vary within only a small range compared to raw values, implying that bias correction is reliable and necessary for these analysis. The variations for Tm, Tmax, Tmin, DTR, FD and HD in future periods and differences between GCMs and PRECIS for 2071–2100 is larger than for 2031–2060 and 1961–1990 (Figs. 2, 5 and 7). This means that the inter-model uncertainty is enlarged in the late 21st century since individual models behave differently in response to identical external forces (Guo et al. 2018a; Wang et al. 2017b). The differences for FD projections among the models tend to be larger with greater warm forcings (Wang et al. 2017b) so that the uncertainty between models deserves special attention. One reason for these differences is the inherited uncertainties that originate from emission scenarios and GCM parameterization schemes that can be reduced by the downscaling method but cannot be totally removed (Ning et al. 2012). Another reason is that there is the assumption that the trend will be consistent in the future periods when bias correction is processed. In fact, the future projections are very sensitive to the present climate bias of a model but the inter-relationships are highly nonlinear and dependent (Liu et al. 2013). A potentially better way to optimize the difference is to take ensemble usage including performance-based and equal-weighted ensembles (Wang and Chen 2014; Niu et al. 2018; Zhang et al. 2018). Of course, performance-based ensembles may be more appropriate if the outputs can be distinguished into skillful and unskillful. If not, the equal-weighted ensemble like in the current study can be useful for future models related to climate change assessments.

5 Conclusions

We use the ensemble of top five well-performing models selected from statistical downscaled GCMs and bias corrected PRECIS for each climatic zone. Future projections for temperatures are systematically analyzed in detail to explore regional characteristics across mainland China under RCP4.5 and RCP8.5 scenarios. It is found that:

1) The future warming rate across the whole of mainland China are likely to reach 0.64 ^{o}C per decade and the respective potential rate of FE and HE reach −4442 and 3557 day·km^2 per decade under RCP8.5, about twice that under RCP4.5.

2) The warming increments are higher in the Tibetan Plateau and northern China including Xinjiang, Northeast China, the eastern part of northwest China, Inner Mongolia and North China. The DTR generally decreases and is attributed to a more rapid increase in minimum relative to maximum temperatures. Additionally, a higher value but downward trend in FE is expected in these zones suggesting the current colder areas warm up much faster.

3) In contrast to the Tibetan Plateau and northern China, a lower increment in temperatures and upward trend in DTR are projected in southern China including Huanghuai, Jianghuai, Jianghan, the south Yangzi River, South China and Southwestern China. A higher value and upward rate in HE is highlighted in Jianghuai, Jianghan, the south Yangzi River and South China which are prone to heat stress that are more severe in the future.

Mainland China is very likely to be faced with a general future warming, implying that GHG mitigation is necessary and indispensable in response to climate warming. Moreover, warming changes are different among climatic zones especially for southern and northern parts that have contrary trends suggesting the further exploration of mitigation and adaptation for these specific vulnerable regions.

Declarations

Conflict of interest The authors declare no competing interests.

Funding statement This study is co-funded by Key Projects of China's national twelfth 5-year Science & Technology Pillar Program [2013BAC09B04] and the Key 948 Project [2011-G9].

Authors' contribution Lei Zhang and Yinlong Xu conceive the topic of the work. Chunchun Meng and Yuncheng Zhao archive the datasets and draw the figures. Lei Zhang drafts the manuscript, Yinlong Xu and Changgui Wang revise the manuscript.

Availability of data and material The datasets used during the current study are available from the corresponding author on reasonable request.

Code availability Available on request.

Ethics approval Not applicable.

Consent to participate Not applicable.

Consent for publication The author gives consent to the publication of all details of the manuscript, including texts, figures, and tables.

References

1. Bannister D, Herzog M, Graf HF, Hosking JS, Short CA (2018) An assessment of recent and future temperature change over the Sichuan Basin, China, using CMIP5 climate models. J Clim 30:6701-6722, https://doi.org/10.1175/JCLI-D-16-0536.1.
2. Bürger G, Murdock TQ, Werner AT, Sobie SR, Cannon AJ (2012) Downscaling extremes-An intercomparison of multiple statistical methods for present climate. J Clim 25:4366-4388, https://doi.org/10.1175/JCLI-D-11-00408.1.
3. Challinor AJ, Watson J, Lobell D, Howden SM, Smith DR, Chhetri N (2014) A meta-analysis of crop yield under climate change and adaptation. Nat Clim Change, 4:287-291, https://doi.org/10.1038/nclimate2153.
4. Chen L, Frauenfeld OW (2014) Surface air temperature changes over the twentieth and twenty-first centuries in China simulated by 20 CMIP5 models. J Clim 27:3920-3937, https://doi.org/10.1175/jcli-d-13-00465.1.

5. Chen WL, Jiang ZH, Laurent (2011) Probabilistic projections of climate change over China under the SRES A1B scenario using 28 AOGCMs. J Clim 24:4741-4756, https://doi.org/10.1175/2011JCLI4102.1.
6. Chen X, Zhou T (2016) Uncertainty in crossing time of 2 ^{o}C warming threshold over China. Sci Bull 61:1451-1459, https://doi.org/10.1007/s11434-016-1166-z.
7. Fischer EM, Knutti R (2013) Robust projections of combined humidity and temperature extremes. Nat Clim Change 3:126-130, https://doi.org/10.1038/nclimate1682.
8. Gao XJ, Wang ML, Giorgi F (2013) Climate change over China in the 21st century as simulated by BCCCSM1.1-RegCM4.0. Atmos Ocean Sci Lett 6:381-386, https://doi.org/10.3878/j.issn.1674-2834.13.0029.
9. Gao XJ, Shi Y, Han ZY, Wang ML, Wu J, Zhang DF (2017) Performance of RegCM4 over major river basins in China. Adv Atmos Sci 34:441-455, https://doi.org/10.1007/s00376-016-6179-7.
10. Guo EL, Zhang JQ, Wang YF, Quan L, Zhang R, Zhang F, Zhou M (2019) Spatiotemporal variations of extreme climate events in Northeast China during 1960-2014. Ecological Indicators 96:669-683, https://doi.org/10.1016/j.ecolind.2018.09.034.
11. Guo JH, Huang GH, Wang XQ, Li YP, Lin QG (2018a) Dynamically-downscaled projections of changes in temperature extremes over China. Clim Dyn 50:1045-1066, https://doi.org/10.1007/s00382-017-3660-7.
12. Guo LY, Gao Q, Jiang ZH, Li L (2018b) Bias correction and projection of surface air temperature in LMDZ multiple simulation over central and eastern China. Adv Atmos Sci 9:81-92, https://doi.org/10.1016/j.accre.2018.02.003.
13. Huang DP, Zhang L, Gao G, Sun S (2018) Projected changes in population exposure to extreme heat in China under a RCP8.5 scenario. J Geogr Sci 28:1371-1384, https://doi.org/10.1007/s11442-018-1550-5.
14. IPCC (1992) Climate Change 1992: Supplementary Report to the IPCC Assessment. Cambridge and New York: Cambridge University Press.
15. IPCC (1995) Climate Change 1995: The Science of Climate Change. Contribution of Working Group to the Second Assessment Report of the Intergovernmental Panel on Climate Change. Cambridge and New York: Cambridge University Press.
16. IPCC (2007) Climate Change 2007: The Physical Science Basis. Contribution of Working Group to the Fourth Assessment Report of the Intergovernmental Panel on Climate Change(IPCC). Cambridge and New York: Cambridge University Press.
17. IPCC (2013) Climate change 2013: The physical science basis. Contribution of Working Group I to the Fifth Assessment Report of the Intergovernmental Panel on Climate Change. Cambridge University Press: Cambridge, United Kingdom and New York, NY, USA,.
18. IPCC (2014): Impacts, Adaptation, and Vulnerability. Part B: Regional Aspects. Contribution of Working Group II to the Fifth Assessment Report of the Intergovernmental Panel on Climate Change. Cambridge Univesity Press, Cambridge, United Kingdom and New York.
19. IPCC (2019) Summary for Policymakers. In: Climate Change and Land: an IPCC special report on climate change, desertification, land degradation, sustainable land management, food security, and greenhouse gas fluxes in terrestrial ecosystems.Ji, Z. M. and S. C. Kang, 2015: Evaluation of extreme climate events using a regional climate model for China. Int. J. Climatol, 35, 888-902, https://doi.org/10.1002/joc.4024.
20. Jiang DB, Zhang Y, Sun JQ (2009) Ensemble projection of 1-3^{o}C warming in China. Chin Sci Bull 54:3326-3334, https://doi.org/10.1007/s11434-009-0313-1.
21. Jiang ZH, Song J, Li L, Chen WL, Wang ZF, Wang J (2012) Extreme climate events in China: IPCC-AR4 model evaluation and projection. Climatic Change 110:385-401 https://doi.org/10.1007/s10584-011-0090-0.
22. Jones B, O'neill BC, Mcdaniel L, Mcginnis S, Mearns LO, Tebaldi C (2015) Future population exposure to US heat extremes. Nat Clim Change 5:652-655, https://doi.org/10.1038/nclimate2631.
23. Kukal MS, Irmak S (2018) U.S. Agro-Climate in 20th century: Growing degree days, first and last frost, growing season length, and impacts on crop yields. Sci Rep 8:6977, https://doi.org/10.1038/s41598-018-25212-2.
24. Li XH, Xu YL, Meng CC, Zhang L, Wang CG (2018a) Analysis on the changes of agro-meteorological thermal indices in Northeast China under RCP4.5 scenario using the PRECIS2.1. Atmosphere 9:323, https://doi.org/10.3390/atmos9080323.
25. Li Y, Ren T, Kinney P, Joyner A, Zhang W (2018b) Projecting future climate change impacts on heat-related mortality in large urban areas in China. Environ Res 163:171-185, https://doi.org/10.1016/j.envres.2018.01.047.
26. Li ZG, Liu ZH, Anderson W, Yang P, Wu WB (2015) Chinese rice production area adaptations to climate changes, 1949-2010. Environ Sci Technol 49:2032-2037, https://doi.org/10.1021/es505624x.
27. Liang XZ, Sun C, Zheng XH, Dai YH, Xu M, Choi HI, Ling TJ, Qiao FX, Kong XH, Bi XQ, Song LC, Wang F (2019) CWRF performance at downscaling China climate characteristics. Clim Dyn 52:2159-2184, https://doi.org/10.1007/s00382-018-4257-5.
28. Lin L, Wang ZL, Xu YY, Zhang X, Zhang H, Dong W (2018) Additional intensification of seasonal heat and flooding extreme over China in a 2°C warmer world compared to 1.5°C. Earth's Future 6:968-978, https://doi.org/10.1029/2018EF000862.
29. Liu Q, Piao SL, Janssens IA, Fu YS, Peng SS, Lian X, Ciais P, Myneni RB, Peñuelas J, Wang T (2018) Extension of the growing season increases vegetation exposure to frost. Nat Commun 9:426, https://doi.org/10.1038/s41467-017-02690-y.
30. Liu S, Gao W, Liang X (2013) A regional climate model downscaling projection of China future climate change. Clim Dyn 41:1871-1884, https://doi.org/10.1007/s00382-012-1632-5.
31. Marotzke J, Jakob C, Bony S, Dirmeyer PA, O'gorman PA, Hawkins E, Perkins-Kirkpatrick S, Quéré CL, Nowicki S, Paulavets K, Seneviratne SI, Stevens B, Tuma M (2017) Climate research must sharpen its view. Nat Clim Change 7:89-71, https://doi.org/10.1038/nclimate3206.

32. Massey N, Jones R, Otto FEL, Aina T, Wilson S, Murphy JM, Hassell D, Yamazaki YH, Allen MR (2015) Weather@home-development and validation of a very large ensemble modelling system for probabilistic event attribution. Q J R Meteorol Soc 141:1528-1545, https://doi.org/10.1002/qj.2455.
33. Ning L, Mann ME, Crane R, Wagener T, Jr RGN, Singh R (2012) Probabilistic projections of anthropogenic climate change impacts on precipitation for the mid-Atlantic region of the United States. J Clim 25:5273-5291, https://doi.org/10.1175/JCLI-D-11-00565.1.
34. Ning L, Riddle EE, Bradley RS (2015) Projected changes in climate extremes over the northeastern United States. J Clim 28:3289-3310, https://doi.org/10.1175/JCLI-D-14-00150.1.
35. Niu X, Wang S, Tang J, Lee DK, Gutowski K, Dairaku W, Mcgregor J, Katzfey J, Gao X, Wu J, Hong SY, Wang Y, Sasaki H, Fu C (2018) Ensemble evaluation and projection of climate extremes in China using RMIP models. Int J Climatol 38:2039-2055, https://doi.org/10.1002/joc.5315.
36. Russo S, Sterl A (2011) Global changes in indices describing moderate temperature extremes from the daily output of a climate model. J Geogr Sci Atmos 116:D03104, https://doi.org/10.1029/2010JD014727.
37. Sen P K (1968) Estimates of the regression coefficient based on Kendall' s tau. J Amer Statistical Assoc 63:1379-1389, https://doi.org/10.1080/01621459.1968.10480934.
38. Shi J, Cui L, Wang J, Du H, Wen K (2019) Changes in the temperature and precipitation extremes in China during 1961-2015. Quat Int 527:64-78, https://doi.org/10.1016/j.quaint.2018.08.008.
39. Sun XB, Ren GY, You QL, Ren YY, Xu WH, Xue XY, Zhan YJ, Zhang SQ, Zhang PF (2019) Global diurnal temperature range (DTR) changes since 1901. Clim Dyn 52:3343-3356, https:// doi.org/10.1007/s00382-018-4329-6.
40. Sylla MB, Faye AG, Diedhiou F, Kunstmann H (2018) Projected heat stress under 1.5 °C and 2 °C global warming scenarios creates unprecedented discomfort for humans in West Africa. Earth's Future 6:1029-1044, https://doi.org/10.1029/2018EF000873.
41. The Third National Assessment Report on Climate Change Editorial Committee (2015) Third National Assessment Report on Climate Change. Beijing: Science Press.
42. Thiel H (1950) A rank-invariant method of linear and polynomial regression analysis, Part 3. Proceedings of Koninalijke Nederlandse Akademie van Weinenschatpen A 53:1397-1412, https://doi.org/10.1007/978-94-011-2546-8_20.
43. Tian D, Yan G,. Dong WJ (2015) Future changes and uncertainties in temperature and precipitation over China based on CMIP5 models. Adv Atmos Sci 32:487-496, https://doi.org/10.1007/s00376-014-4102-7.
44. Wang L, Chen W (2014) A CMIP5 multimodel projection of future temperature, precipitation, and climatological drought in China. Int J Climatol 34:2059-2078, https://doi.org/10.1002/joc.3822.
45. Wang QX, Wang MB, Fan XH, Zhang F, Zhu SZ, Zhao TL (2017a) Trends of temperature and precipitation extremes in the Loess Plateau Region of China,1961-2010. Theor Appl Climatol 129:949-963, https://doi.org/10.1007/s00704-016-1820-z.
46. Wang XX, Jiang DB, Lang XM (2017b) Future extreme climate changes linked to global warming intensity. Sci Bull 62:1673-1680, https://doi.org/10.1016/j.scib.2017.11.004.
47. Wang Y, Sun Y, Hu T, Song LC (2017c) Attribution of temperature changes in Western China. Int J Climatol 38:742-750, https://doi.org/10.1002/joc.5206.
48. Werner AT, Cannon AJ (2015) Hydrologic extremes-an intercomparison of multiple gridded statistical downscaling methods. Hydrol. Earth Syst Sci 12:6179-6239, https://doi.org/10.5194/hess-20-1483-2016.
49. Xu YL, Zhang Y, Lin YH, Lin ED, Lin WT, Dong WJ, Richard J, David H, Simon W (2006) Analysis of response to climate change in China under SRES B2 scenario using PRECIS. Chinese Sci Bull 51:2068-2074, https://doi.org/10.1360/csb2006-51-17-2068.
50. Xu K, Wu C, Hu B (2019) Projected changes of temperature extremes over nine major basins in China based on the CMIP5 multimodel ensembles. Stoch Env Res Risk A 33:321-339, https://doi.org/10.1007/s00477-018-1569-2,
51. Xu Y, Gao XJ, Giorgi F (2010) Upgrades to the reliability ensemble averaging method for producing probabilistic climate-change projections. Clim Res 41:61-81, https://doi.org/10.3354/cr00835.
52. Xu YP, Zhang X, Ran Q, Tian Y (2013) Impact of climate change on hydrology of upper reaches of Qiantang River Basin, East China. J Hydrol 483:51-60, https://doi.org/10.1016/j.jhydrol.2013.01.004.
53. Yang SL, Feng JM, Dong WJ, Chou J (2014) Analyses of extreme climate events over China based on CMIP5 historical and future simulations. Adv Atmos Sci 31:1209-1220, https://doi.org/10.1007/s00376-014-3119-2.
54. Yang HL, Xu YL, Zhang L, Pan J, Li X (2010) Projected change in heat waves over China using the PRECIS climate model. Clim Res 42:79-88, https://doi.org/10.3354/cr00860.
55. You QL, Wang D, Jiang ZH, Kang SC (2017) Diurnal temperature range in CMIP5 models and observations on the Tibetan Plateau. Q J R Meteor Soc 143:1978-1989, https://doi.org/10.1002/qj.3057.
56. Yue TX, Zhao N, Fan ZM, Li J, Chen CF, Lu YM, Wang CL, Xu B, Johnwilson (2016) CMIP5 downscaling and its uncertainty in China. Glob Planet Change 146:30-37, https://doi.org/10.1016/j.gloplacha.2016.09.003.
57. Zhai YY, Huang G, Wang XQ, Zhou X, Lu C, Li Z (2019) Future projections of temperature changes in Ottawa, Canada through stepwise clustered downscaling of multiple GCMs under RCPs. Clim Dyn 52:3455-3470, https://doi.org/10.1007/s00382-018-4340-y.
58. Zhang YJ, Fu L, Pan J, Xu YL (2017) Projected changes in temperature extremes in China using PRECIS. Atmosphere 8:15, https://doi.org/10.3390/atmos8010015.
59. Zhang L,. Yang BY, Li S, Hou Y, Huang DP (2018) Potential rice exposure to heat stress along the Yangtze River in China under RCP8.5 scenario. Agr Forest Meteorol 248:185-196, https://doi.org/10.1016/j.agrformet.2017.09.020.

60. Zhang L, Xu YL, Meng CC, Li XH, Wang CG (2020) Comparison of statistical and dynamic downscaling techniques in generating high-resolution temperature in China from CMIP5 GCMs. J Appl Meteorol Clim 59:207-235, https://doi.org/10.1175/JAMC-D-19-0048.1.
61. Zhang Q, Li J, David CY, Chen X (2011) Observed changes of temperature extremes during 1960-2005 in China: natural or human-induced variations? Theor Appl Climatol 106:417-431, https://doi.org/10.1007/s00704-011-0447-3.
62. Zhang S, Tao FL, Zhang Z (2014) Rice reproductive growth duration increased despite of negative impacts of climate warming across China during 1981-2009. Eur J Agrono 54:70-83, https://doi.org/10.1016/j.eja.2013.12.001.
63. Zhao C, Piao SL, Huang Y, Wang X, Ciais P, Huang M, Zeng Z, Peng S (2016) Field warming experiments shed light on the wheat yield response to temperature in China. Nat Commun 7:13530, https://doi.org/10.1038/ncomms13530.
64. Zhou B, Wen QH, Xu Y, Song LC, Zhang X (2014) Projected changes in temperature and precipitation extremes in China by the CMIP5 multimodel ensembles. J Clim 27:6591-6611, https://doi.org/10.1175/jcli-d-13-00761.1.
65. Zhou X, Huang GH, Wang XQ, Chen GH (2018) Dynamically-downscaled temperature and precipitation changes over Saskatchewan using the PRECIS model. Clim Dyn 50:1321-1334, https://doi.org/10.1007/s00382-017-3687-9.
66. Zhu JX, Huang G, Wang XQ, Cheng GH (2017) Investigation of changes in extreme temperature and humidity over China through a dynamical downscaling approach. Earth Future 5:1136-1155, https://doi.org/10.1002/2017EF000678.
67. Zhu XH, Wang WQ, Fraedrich K (2013) Future climate in the Tibetan Plateau from a statistical regional climate model. J Clim 15:10125-10138, https://doi.org/10.1175/JCLI-D-13-00187.1.

Figures

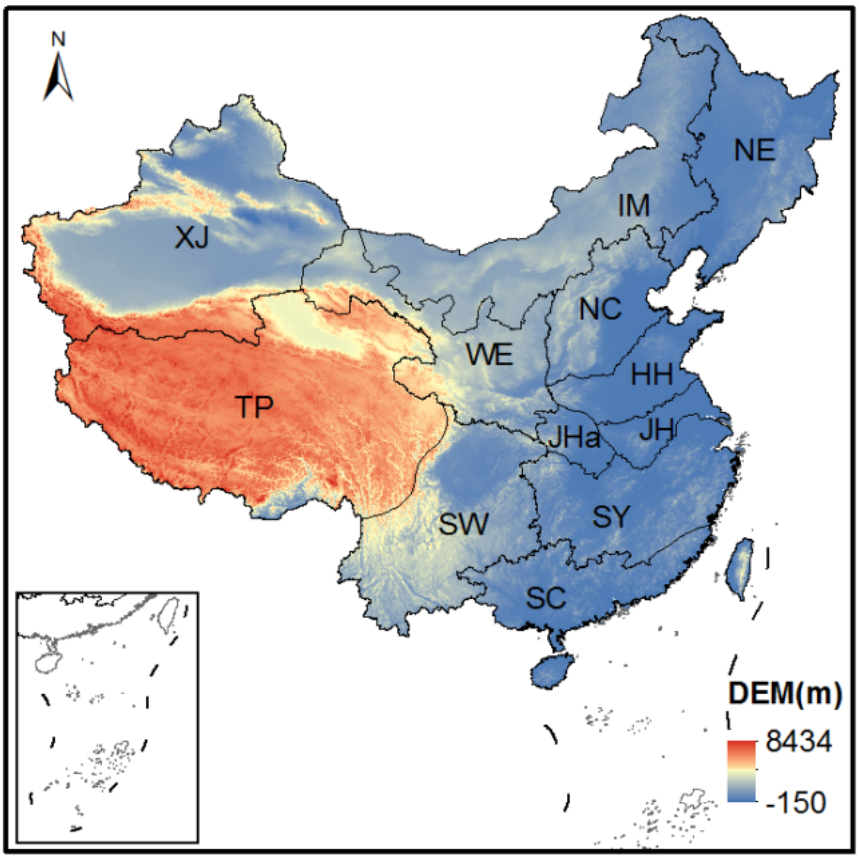

Figure 1

The location of study region (DEM is Digital Elevation Model)

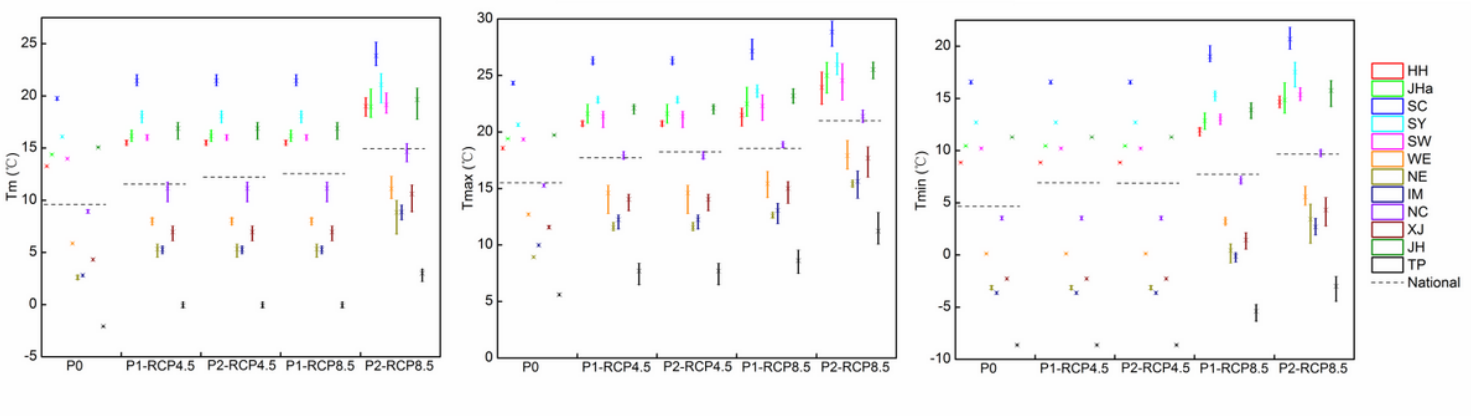

Figure 2

Variation of Tm, Tmax and Tmin different periods (P0, P1 and P2 represent 1961-1990, 2031-2060 and 2071-2100, respectively; Colored bars show the variation between models; Dashed horizontal line represent the mean value in the whole of mainland China)

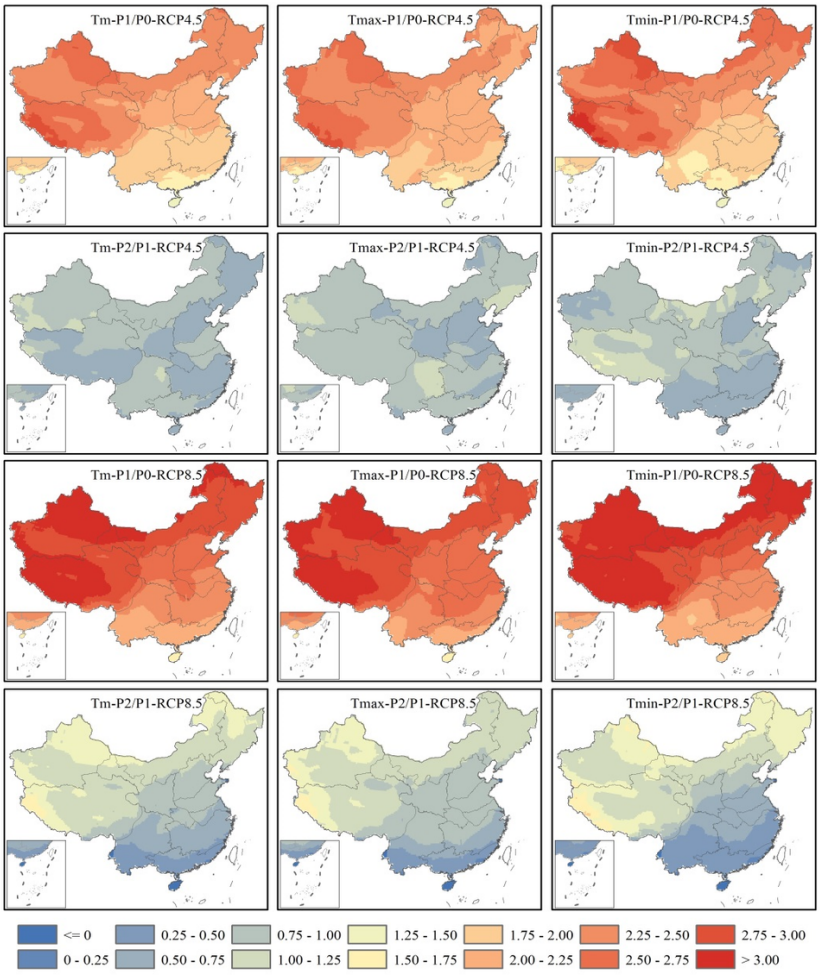

Figure 3

Change of Tm, Tmax and Tmin between different periods (P0, P1 and P2 represent 1961-1990, 2031-2060 and 2071-2100, respectively; P1/P0 and P2/P1 represent the value of P1 minus P0 and P2 minus P1)

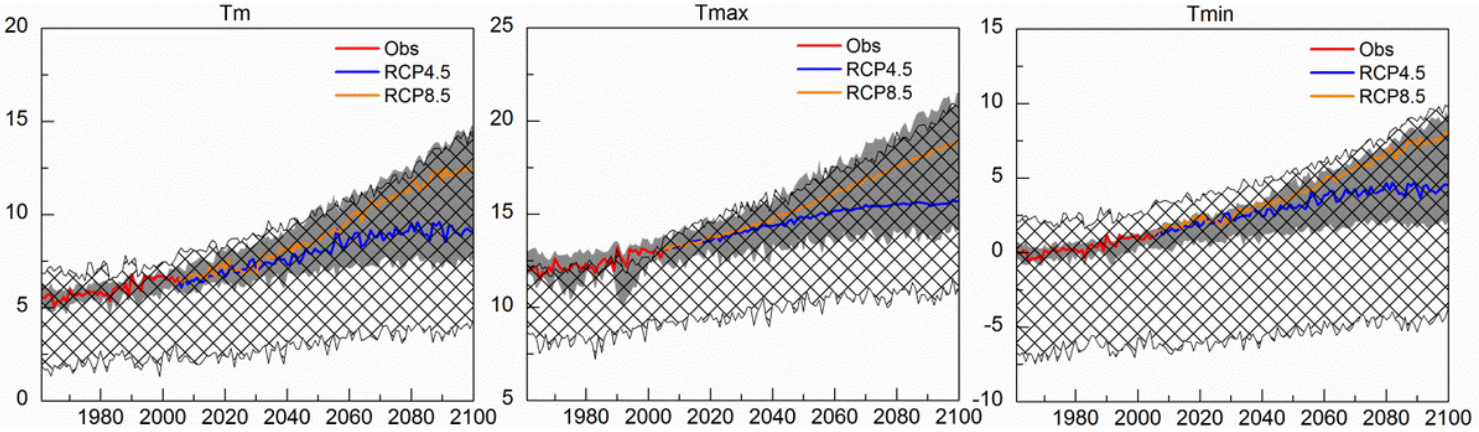

Figure 4

Variation of Tm, Tmax and Tmin with year (Red line, blue line, orange line, shaded area and gridded area indicate the ensemble of all models in the observed period, ensemble of all models under RCP4.5, ensemble of all models under RCP8.5, range of bias corrected models and range of raw models, respectively)

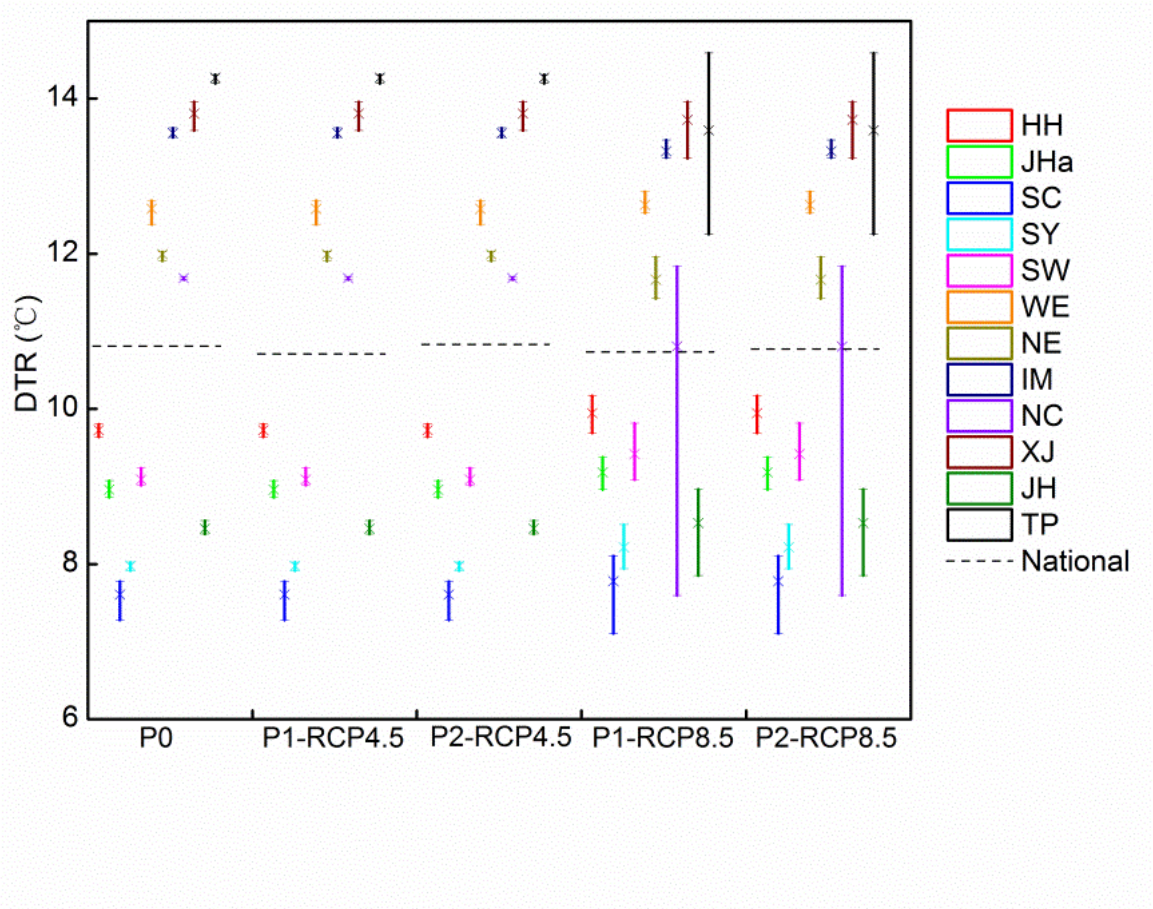

Figure 5

Variation of DTR during different periods (P0, P1 and P2 represent 1961-1990, 2031-2060 and 2071-2100, respectively; Colored bars show the variation between models; Dashed horizontal line represent the mean value in the whole of mainland China)

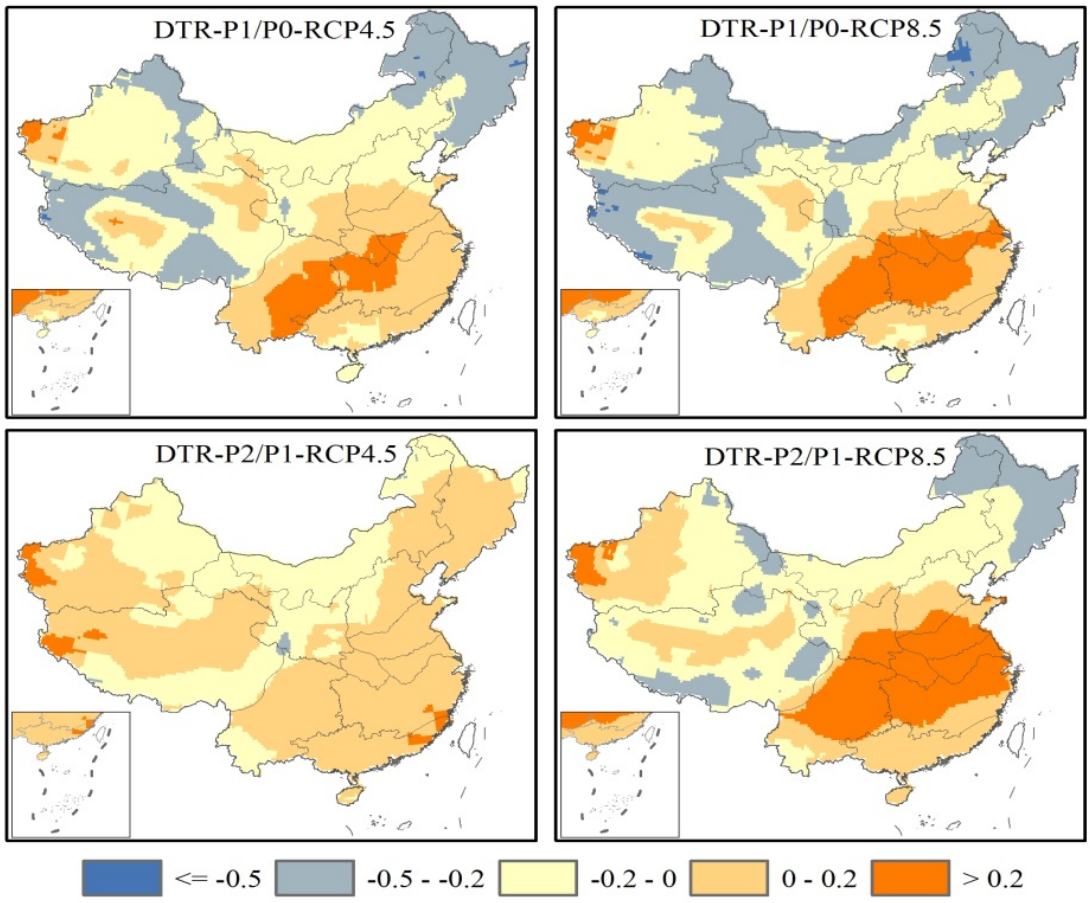

Figure 6

Change of DTR between different periods (P0, P1 and P2 represent 1961-1990, 2031-2060 and 2071-2100, respectively; P1/P0 and P2/P1 represent the value of P1 minus P0 and P2 minus P1)

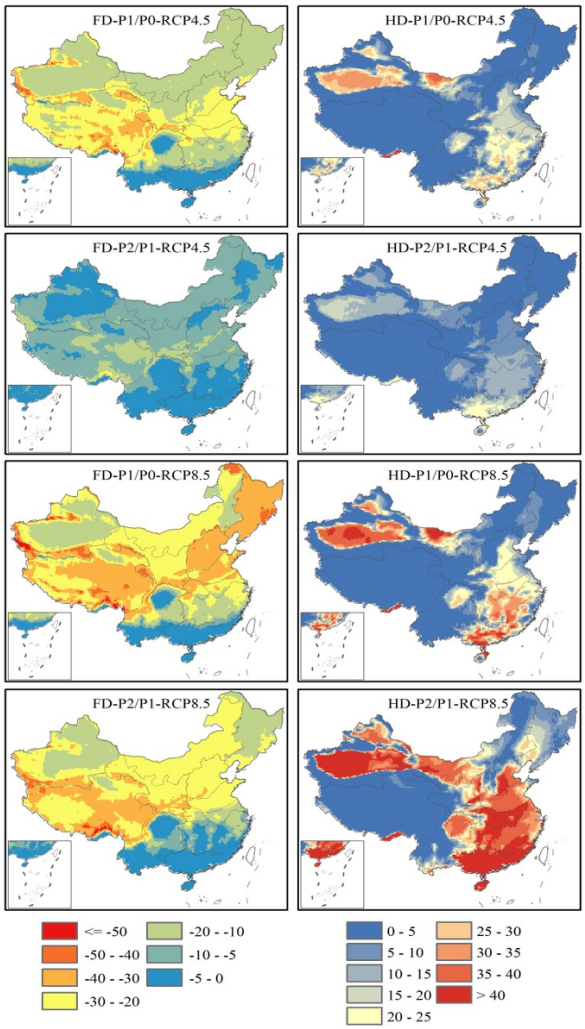

Figure 7

Change of FD and HD between different periods (P0, P1 and P2 represent 1961-1990, 2031-2060 and 2071-2100, respectively; P1/P0 and P2/P1 represent the value of P1 minus P0 and P2 minus P1)

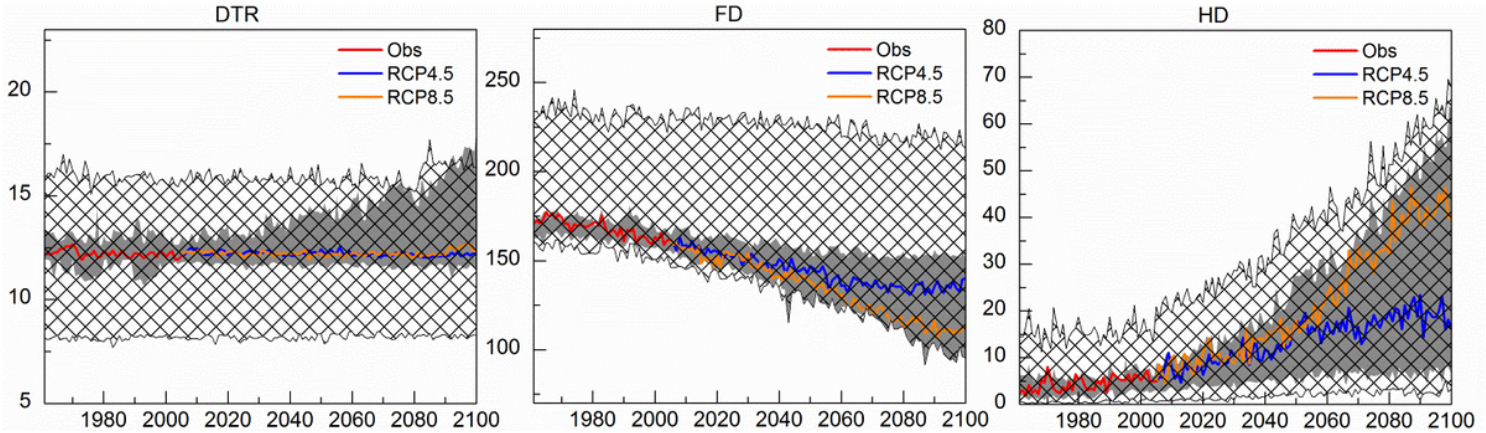

Figure 8

Variation of DTR, FD and HD with year (Red line, blue line, orange line, shaded area and gridded area indicate the ensemble of all models in the observed period, ensemble of all models under RCP4.5, ensemble of all models under RCP8.5, range of bias corrected models and range of raw models, respectively)

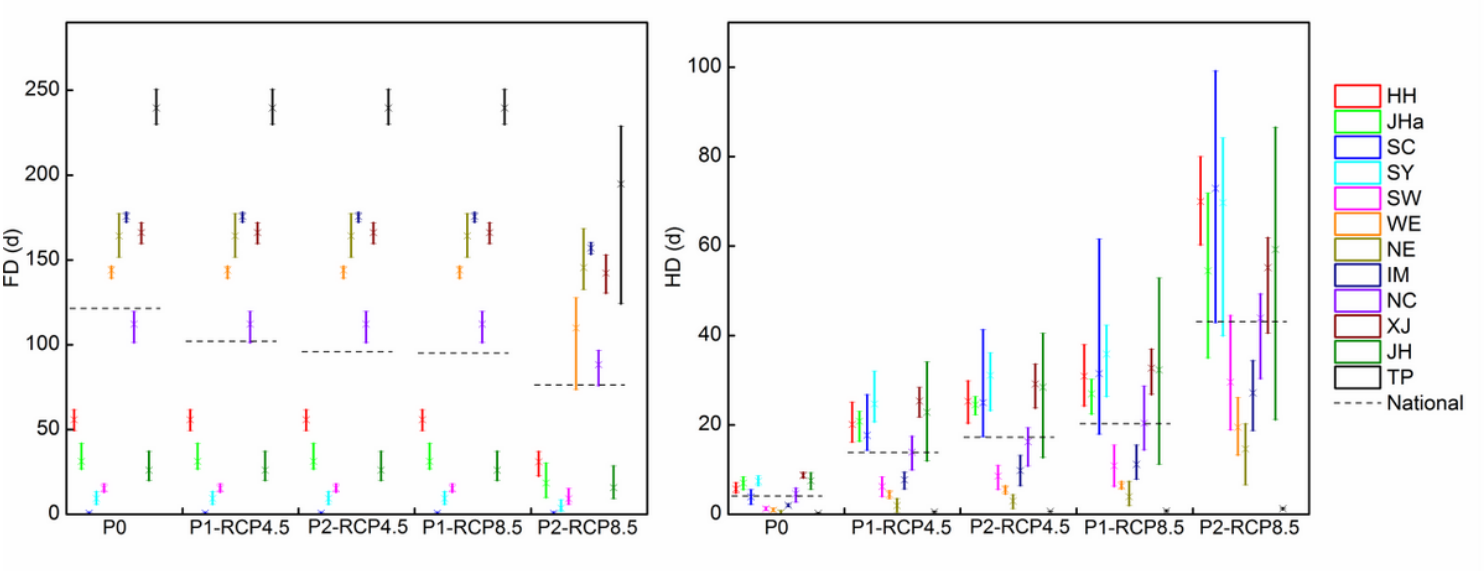

Figure 9

Variation of FD and HD during different periods (P0, P1 and P2 represent 1961-1990, 2031-2060 and 2071-2100, respectively; Colored bars show the variation between models; Dashed horizontal line represent the mean value in the whole of mainland China)

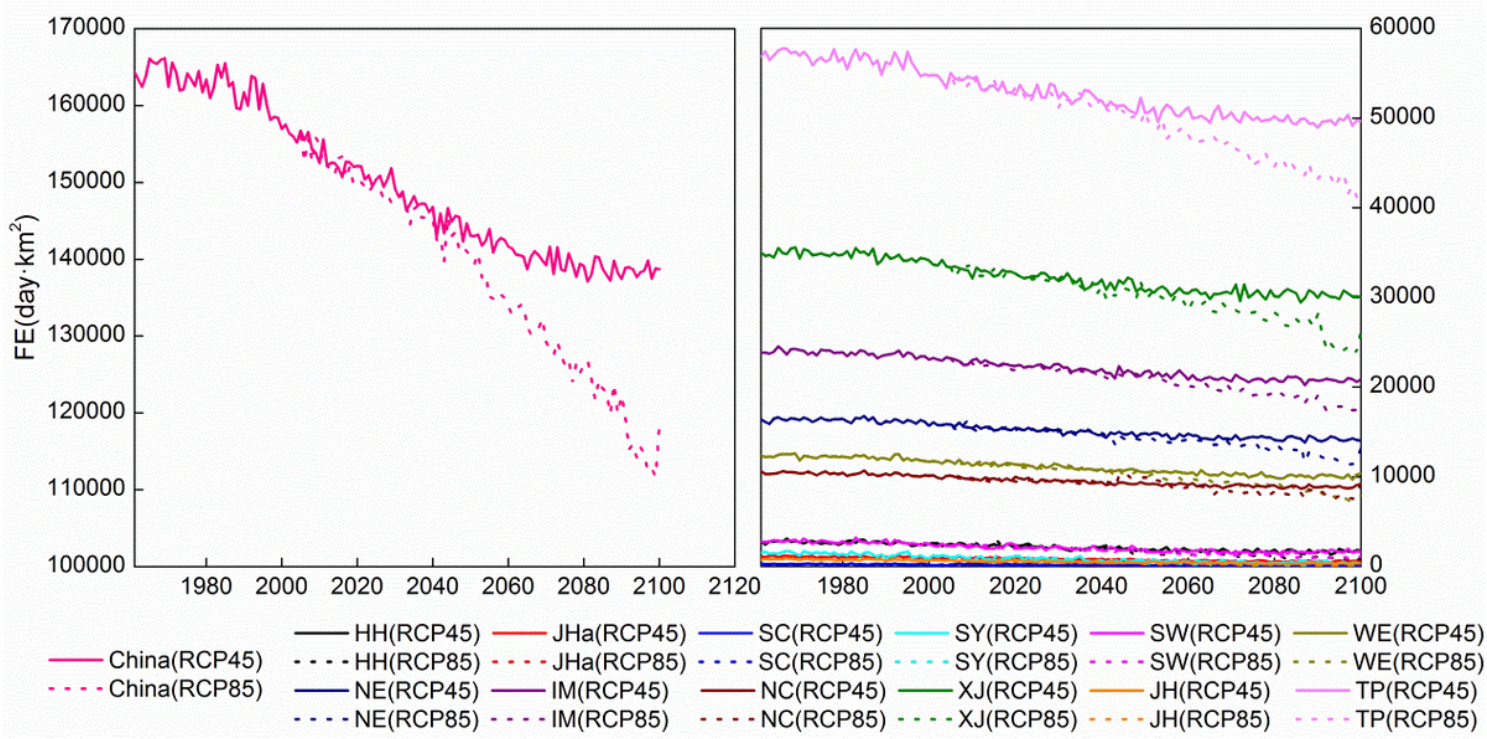

Figure 10

Yearly change of FE across the whole of mainland China and regions

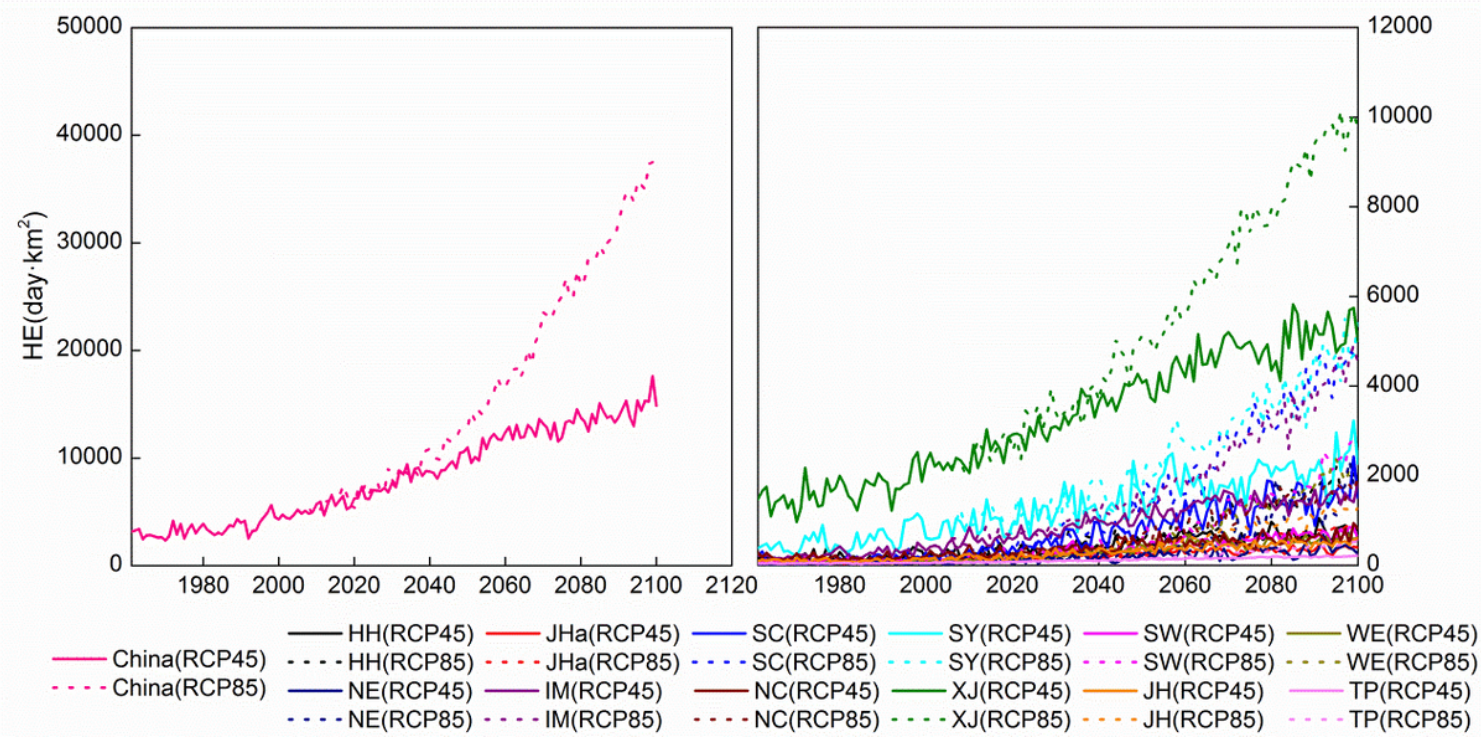

Figure 11

Yearly change of HE across the whole of mainland China and regions

Supplementary Files

This is a list of supplementary files associated with this preprint. Click to download.

- Supplements.docx